

On the Feasibility of Out-of-Band Spatial Channel Information for Millimeter-Wave Beam Search

Pekka Kyösti, Peize Zhang, *Member, IEEE*, Aarno Pärssinen, *Senior Member, IEEE*, Katsuyuki Haneda, *Member, IEEE*, Pasi Koivumäki, *Member, IEEE*, and Wei Fan, *Senior Member, IEEE*

Abstract—Prolonged beam alignment is the main source of overhead in mobile wireless communications at millimeter-wave (mm-wave) frequencies due to narrow beams following the requirement of high antenna gains. Out-of-band spatial information may be used in initial beam search when lower frequency band radios are operating in conjunction with mm-wave radios. The feasibility of using low-band channel information for coarse estimation of high-band beam directions strongly depends on the spatial congruence between the two frequency bands. In this work, we try to answer two related questions. First, how similar is the power angular spectrum (PAS) of propagation channels between two widely separated frequency bands? Then, what is the impact of practical antenna configurations on spatial channel similarity? We propose a beam directions based metric to assess the power loss and number of false directions if out-of-band spatial information is used instead of in-band information. This metric is more practical and useful than comparing the PASs directly. Point cloud ray tracing and propagation measurement results across multiple frequency bands and environments are used to show that the degree of spatial similarity of beamformed channels is related to antenna beam widths, frequency gap, and radio link conditions.

Index Terms—Beam search, millimeter-wave, radio channel, spatial channel similarity.

I. INTRODUCTION

AS THE global adoption of 5G technology continue, next generation wireless communication systems, i.e., B5G/6G are expected to provide ultra-high throughput and seamless connectivity in coexisting sub-6 GHz and millimeter-wave (mm-wave) cellular networks [1]. Following the reasoning and definitions of [2], we divide the mm-wave radio frequency (RF) as the lower region, 30–100 GHz, and the

upper region, 100–300 GHz, and name them the lower and the upper mm-wave band, respectively. The transmission loss increases with increasing frequency and, typically, higher antenna gains are used to compensate for the losses. A few dBi might not be sufficient anymore, but antenna gains of even a few tens of decibels might be needed at the upper mm-wave RF [3]. The gain may be realized by, e.g., high gain antenna elements, lens structures, phased arrays, or combinations of these [3]. Here we assume flexible beam steering capability and hence phased arrays.

From the propagation analysis perspective, high-capacity mm-wave cellular communications will likely offer up to a few hundred meters of directed coverage [4], [5]. Supported link distances become substantially shorter in non-line of sight (NLOS) scenario [6], [7], because of severe path loss and sensitivity to blockage due to obstacles. Apart from the frequency and distance dependent free space path loss, also the losses related to diffraction and material penetration strongly increase with increasing frequency [8], while the reflection coefficients are rather constant across sub-6 GHz and mm-wave frequencies. Attenuation of paths due to shadowing by obstacles becomes stronger at higher RF. The probability of blockage on one hand may increase, since with shorter wavelengths the Fresnel zone becomes smaller and even smaller obstacles may block the path. While on the other hand, smaller openings between obstacles are needed to keep smaller Fresnel zones non-obstructed [2]. Another type of blocking of signals, i.e., interference by other radio sources, will be less severe due to more directive antennas and focused beams.

Higher antenna gain means practically more directivity and narrower beams of radiation patterns. Initialization of a communication link with transceivers relying on adaptive high-gain antenna systems necessitates a beam search procedure [9]. A high gain antenna, forming a narrow beam, is susceptible to loss of signal, leading to a more laborious beam search scheme [10]. Overall, the higher the RF the more carefully narrow antenna beams must be directed and the more frequently severe blockage events will occur, especially if antennas are on low height and there is motion either by transceivers or the environment. Sub-6 GHz radio systems can establish more flexible and reliable communication links with continuous coverage, as compared to mm-wave systems. Coming B5G/6G transceivers are foreseen to support multi-band transmission across a wide set of frequencies. Therefore, it is attractive to reuse available out-of-band spatial channel information for higher frequency beam steering and alignment with reduced training overhead [11], [12]. I.e., extracting

Manuscript received 17 October 2022; revised 1 February 2023; accepted 15 February 2023. Date of publication ; date of current . This work was partly supported by the European Commission through the H2020 project Hexa-X (Grant no. 101015956) and partly by 6G Flagship programme, funded by Academy of Finland (Grant no. 346208). (*Corresponding author: Pekka Kyösti.*)

Pekka Kyösti is with the Centre for Wireless Communications, University of Oulu, 90570 Oulu, Finland, and also with Keysight Technologies Finland Oy, 90630 Oulu, Finland (e-mail: pekka.kyosti@oulu.fi).

Peize Zhang and Aarno Pärssinen are with the Centre for Wireless Communications, University of Oulu, 90570 Oulu, Finland (e-mail: peize.zhang; aarno.parssinen@oulu.fi).

Katsuyuki Haneda and Pasi Koivumäki are with the Department of Electronics and Nanoengineering, Aalto University, 02150 Espoo, Finland (e-mail: katsuyuki.haneda; pasi.koivumaki@aalto.fi).

Wei Fan is with the Antenna, Propagation and Millimeter-Wave Systems Section, Department of Electronic Systems, Faculty of Engineering and Science, Aalborg University, 9220 Aalborg, Denmark (e-mail: wfa@es.aau.dk).

Color versions of one or more of the figures in this paper are available online at <http://ieeexplore.ieee.org>.

Digital Object Identifier

easily available coarse angular information with low frequency antenna systems and using it to initialize beam search at the higher frequency. This is motivated by findings of multi-band measurements, e.g., the ones described in [13] at 6, 30, and 60 GHz, indicating that there can be a substantial similarity in directions of strong propagation path component across radio frequencies.

The radio channel contains both the propagation channel and antennas, i.e., transceivers always see the channel through antennas. Even though dominant propagation paths are often similar at separate frequencies [2], the antenna systems are not. Physical size of transceivers and antenna structures limit the aperture and consequently the achievable electrical size and directivity of antennas. Systems equipped with larger antenna arrays at higher RF have typically much higher angular resolution and are capable of obtaining finer granularity information of, e.g., directions of multi-path components. Therefore, out-of-band information of the radio channel may not differ only due to the differences in wave propagation, but also due to differences in antennas employed in two frequency bands. To this end, our primary task is to explore how similar the propagation channels are at separate frequency bands and how much useful spatial channel information one band can provide to the other. It is also essential to consider practical antenna size limitations when leveraging low-band spatial channel information for high-band beam search.

Frequency dependence of channel parameters has been a topic of interest in the standardization of wave propagation and channel models for many years [14]. Extensive empirical analyses of indoor and outdoor spatial channels have been promoted in literature, where measured power angular delay profiles (PADPs) are presented and compared over multiple frequencies from microwave to mm-wave bands [13], [15]–[19]. Analysis of directional propagation channels reveals that similar dominant paths can be observed in different frequency bands, yet many more weak multi-path components (MPCs) can be detected in lower bands as compared to the higher bands. Meanwhile, it is clear that spatial profiles at mm-wave bands tend to be more specular and sparse. A method proposed in [15] performs rough and quick angle estimation at a lower frequency and reuses the estimated spatial profiles for precious beam operation at high frequency, considering the high similarity of spatial profiles between low and high frequency bands. In [20], channel sounding results reported in mmMAGIC project, covering different propagation scenarios and different frequency bands in 2 to 86 GHz [21], were summarized with the focus on the statistical analysis of delay dispersion parameters. Though multi-band channel similarity can be directly observed, there is a lack of metrics to characterize the degree of it. In [22], a multi-path similarity index was proposed to measure temporal channel similarity by comparing multi-band power delay profiles (PDPs). To the best of our knowledge, however, no definite metric has been proposed to measure the spatial channel similarity in terms of power angular spectrum (PAS).

In this context, this paper provides the following specific contributions.

- Two metrics for the evaluation of spatial channel sim-

ilarity at two different frequencies are developed under practical antenna pattern constraints, where one offers a probability measure on the total variation distance of PAS while the other offers a more practical and intuitive scheme to identify the available beam directions. Compared with existing multi-frequency propagation studies, we not only provide a visual comparison of site-specific spatio-temporal channel characteristics across different frequencies, but also propose quantitative metrics to characterize spatial similarity level of radio channels.

- To conduct a statistical analysis, a sufficient large amount of multi-band propagation channel data at the same transmitter (Tx) and receiver (Rx) locations has been collected. We use point clouds ray tracing, which is an attractive approach given the difficulty of conducting extensive channel measurement campaigns consisting of thousands of locations. In addition, dual-band channel sounding data from a few environments are utilized for validation. Fair comparison of multi-band spatial channel characteristics can be performed at identical Tx-Rx settings.
- Statistical analysis of multi-band spatial channel similarity using our proposed metrics provides valuable insights into the feasibility of out-of-band spatial channel information for mm-wave beam steering and alignment. The usefulness of lower band channel information for mm-wave beam search will change depending on the system configurations, such as antenna configurations, channel line of sight (LOS) condition, and beam direction estimation methods.

The remainder of this paper is organized as follows. Section II introduces the propagation data obtained by point cloud ray tracing simulations and channel measurements across multiple frequency bands and environments. Section III describes two proposed metrics to measure the spatial channel similarity based on the multi-band PAS. Section IV discusses the feasibility of lower frequency spatial channel information aided mm-wave beam search using practical antenna configurations and Section V concludes the paper.

II. MULTI-BAND PROPAGATION CHANNEL DATA COLLECTION

In this section we briefly describe propagation data analysed in later sections.

A. Point Cloud Ray Tracing Simulations

The propagation channel data used in this work is generated via ray tracing simulations in applying a laser-scanned point cloud model of the Helsinki-Vantaa airport check-in area at Terminal 2 [23], [24]. The raw point cloud is obtained with a Z+F IMAGER[®] 5006h 3D laser-scanner [25], which uses movable mirrors to steer a laser beam in different directions to detect the distances to reflective surfaces. The point cloud used in ray tracing simulations is illustrated in Fig. 1(a). Note that the raw point cloud is preprocessed by removing the ceiling of the airport terminal (i.e., points above 10 m), as well as the floor, which will significantly reduce the total number of points for ray tracing simulations. Other clutters,

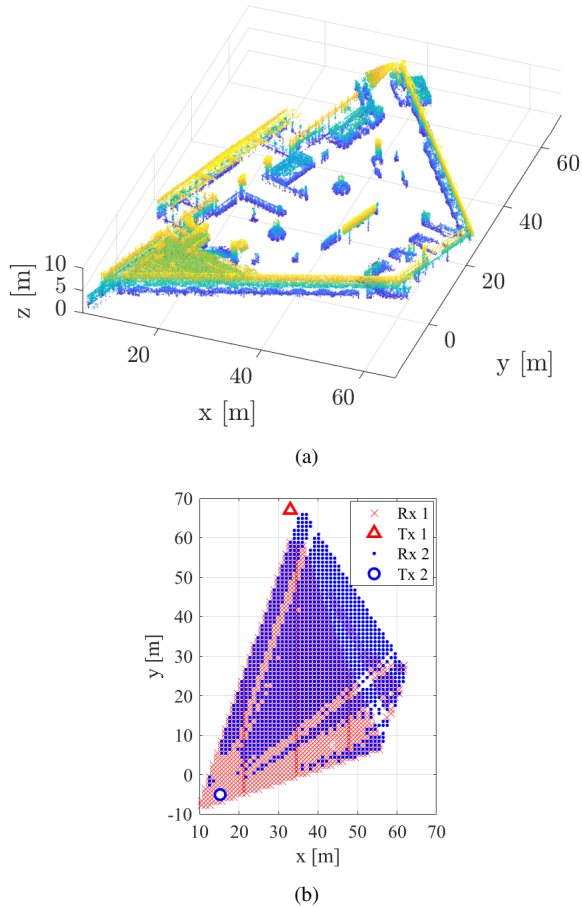


Fig. 1. (a) Laser-scanned point cloud used in ray tracing, where the points are colored according to their position on the z -axis. (b) Tx and Rx positions.

for example, pedestrians that were present during the laser scanning, are removed so that the ray tracing simulations were performed without any human present in the hall. The points that represent the walls of the airport terminal, check-in kiosks, and other fixtures of the environment are kept during ray tracing simulations. As shown in Fig. 1(b), two Tx locations are selected, where Tx1 is in a side corridor and Tx2 is behind the stairs in the check-in area. Two Rx sets are selected, including thousands of Rx locations, to establish communication links to Tx1 and Tx2, respectively. Propagation data contains in total 2875 links, composed of 1473 links between Tx1 and Rx1 and 1402 links between Tx2 and Rx2. It can be observed that Rx locations are not fully uniform since certain sectors with direct paths to the corresponding Rx locations are excluded. Thus, only NLOS links are considered during the simulation, while line-of-sight (LOS) links are all blocked by physical objects.

As regards to the ray tracing simulation setup, the following propagation mechanisms are considered in the simulations, including single- and double-bounce paths, diffracted paths, and diffraction to single and double-bounce paths. Total five frequency bands (i.e., 4, 15, 28, 60, and 86 GHz) are considered. The permittivity of the environment and shadowing losses for each frequency, which were used in the ray tracing simulations, are summarized in Table I. These parameters

TABLE I
RAY TRACING SIMULATION PARAMETERS.

Frequency [GHz]	4	15	28	60	86
Permittivity	4.3	4.2	3.9	3.6	3.3
Shadowing loss [dB]	20	30	60	100	130

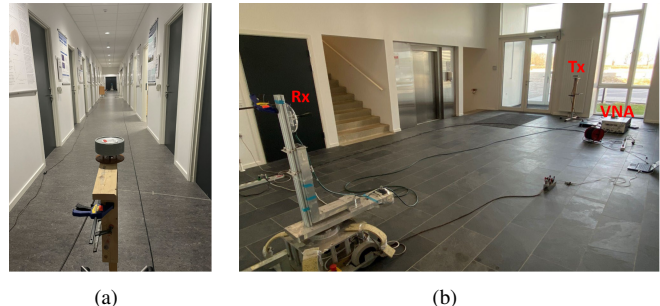


Fig. 2. Channel measurement campaigns in (a) indoor corridor and (b) entrance hall.

are optimized based on the channel measurement campaign conducted at the airport [26] following the methodology outlined in [21]. Note that the measured or optimized parameters were not available at 4 GHz, and they were obtained using a linear fit according to the available parameters in other bands. The permittivity of the physical objects in the environment is assumed to be identical for simplicity of the measurement-based calibration and is used to calculate reflection and diffraction coefficients. A flat shadowing loss, originally estimated from field measurement data, is applied to the rays that are *shadowed*, i.e., whose 1st Fresnel ellipsoid is not free of obstructions [27], [28].

B. Channel Measurement Campaigns

Channel measurements in two indoor scenarios (see Fig. 2) were performed in Aalborg University, Denmark. A long-range vector network analyzer (VNA) based channel sounding system enabled by radio over fiber (RoF) technology was employed for the measurements. The details about the channel sounder at 28 GHz can be found in [29]. In [30], a long-range channel sounder at 220–330 GHz was reported. Same concept is employed for the 100 GHz channel sounder utilized in our measurement, except that different frequency extenders are used. For both channel measurements, omni-directional antennas were used at the Tx side, while directional antennas were employed at the Rx side to cover 360° in the azimuth domain. Directional channel sounding scheme was employed at the Rx side to measure the spatial channel profile directly with the help of the turntable. Note that directional antennas with similar half power beam width (HPBW) were employed to ensure that channel spatial profiles at different frequency bands are not affected by the antenna pattern. The measured PADPs are estimated based on the method proposed in [31], which can be further used to extract MPCs with peak detection algorithm. A dynamic range of 30 dB is set in the measurement results.

Only one LOS link in each environment was selected due to highly time-consuming measurements. For the indoor corridor

TABLE II
ANTENNA CONFIGURATIONS FOR DUAL-BAND CHANNEL MEASUREMENTS.

Envi.	Indoor corridor		Entrance hall	
Freq. range [GHz]	28–30	99–101	28–30	99–101
Freq. point	1001		1001	601
Tx ant. type	Omni.			
Rx ant. type	Horn			
Rx ant. height [m]	0.93	1.25	1.25	
Rx ant. HPBW [deg]	40	40	20.8	16
Rx ant. Gain [dBi]	13.5	13.5	19.5	20.5
Rx rot. Step [deg]	1.5	1	8	8

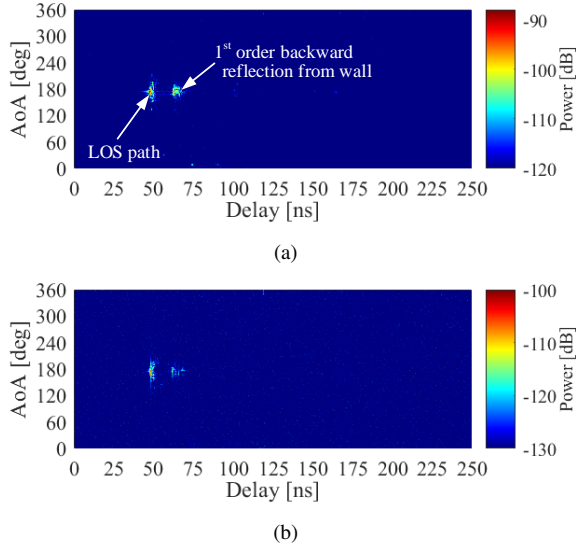


Fig. 3. Measured PADPs in indoor corridor at (a) 28 GHz and (b) 100 GHz.

scenario, a measurement bandwidth of 2 GHz with 1001 frequency points was set in the VNA, resulting in a delay resolution of 0.5 ns and maximum excess delay of 500 ns. The measurement distance was set to 14 m. The measured PADPs at 28 GHz and 100 GHz are shown in Fig. 3. The measured channels are highly sparse and specular, and the same dominant paths along LOS directions can be identified at two frequencies. For the entrance hall scenario, 1001 and 601 frequency points were selected with the same sounding bandwidth of 2 GHz at 28 GHz and 100 GHz, respectively. The measurement distance was set to 4.84 m. The details of antenna configurations are summarized in Table II.

C. Multi-path Channel Characterization

Outputs of the ray tracing and channel measurements include all captured MPCs within a specific power range. Each MPC is characterized by its received power, propagation delay, angle of arrival (AoA), and angle of departure (AoD) (when available). In single directional case, the discrete PADP can be written as $P(q; \Omega, \tau)$, where q denotes the index for the link, i.e., for the Tx and Rx location, Ω denotes the AoA, and τ denotes the propagation delay. In this paper we only analyze the spatial channel similarity on Rx side only, but

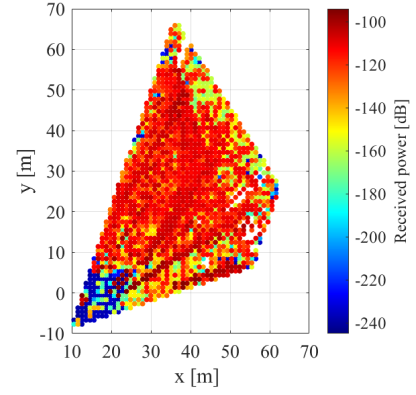


Fig. 4. Total channel gain in each Rx position at 86 GHz.

the same applies to Tx side as well, since Tx and Rx were deployed similarly. For the sake of simplicity, we use subscript L and U to denote the lower and upper frequency antenna systems, propagation channels, and their parameters, respectively. Consequently, each PADP can be represented as a sum of discrete paths $p = 1, \dots, l$ as

$$\begin{cases} P_L(\Omega, \tau) = \sum_{p=1}^{l_L} P_{L,p} \delta(\Omega - \Omega_{L,p}) \delta(\tau - \tau_{L,p}) \\ P_U(\Omega, \tau) = \sum_{p=1}^{l_U} P_{U,p} \delta(\Omega - \Omega_{U,p}) \delta(\tau - \tau_{U,p}), \end{cases} \quad (1)$$

where link index q is left out for brevity, $\delta(\cdot)$ is the delta function, l is the total number of rays, P_p , Ω_p , and τ_p are the received power¹, AoA, and propagation delay of the p th rays, respectively.

Fig. 4 shows the total channel gain of each link at 86 GHz, which is calculated as the sum of channel gains of paths $\sum_{p=1}^l P_p$. A significantly large variation of close to 140 dB in channel gains among different Rx positions can be observed. Discrete PADPs of a specific link at 4 GHz and 86 GHz are shown in Fig. 5, where the circles and triangles represent paths in low and high bands, respectively. In terms of the power difference, the P_p at lower frequency are much larger than those at higher frequency as indicated in Fig. 5(a). It is a bit difficult to explore the channel similarity visually without power normalization. On the other hand, from the top view of 3D PADP (see Fig. 5(b)), dominant rays across two frequencies share similar propagation delays and AoAs. Since our focus in this work is in angular aspects, we reduce PADPs to PASs and mainly treat angular power distributions henceforth.

III. SPATIAL CHANNEL SIMILARITY METRICS

In this section, two metrics used for measuring the spatial channel similarity are proposed based on the multi-band propagation channel data. The first method applies the widely known total variation distance of probability measures on the PAS estimated over different frequency bands. The second method is more practical. There we assume certain antenna

¹We assume unity transmit power and use *received power* and *channel gain* interchangeably.

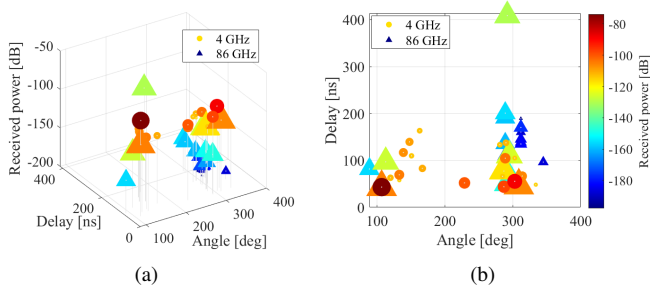


Fig. 5. Comparison of the PADPs at 4 GHz and 86 GHz for link 15. (a) 3D plot. (b) Top view.

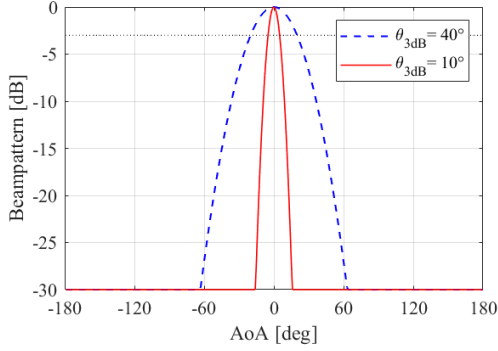


Fig. 6. The normalized gain pattern of the 3GPP beam with $\theta_{3dB} = 10^\circ$ and 40° .

beam widths at different frequencies and try to directly evaluate the usability of spatial channel information extracted at one frequency for the beam search at the other frequency. Following the definitions of two metrics, the comparison study has been conducted across different frequency combinations and methods.

A. PAS Similarity Percentage

An intuitive view of multi-band spatial channel similarity is to directly compare measured PASs. However, a direct comparison of possibly discrete and sparse PASs is difficult. Hence we develop a metric, so-called PAS similarity percentage (PSP), to measure the total variation distance of normalized PASs. According to procedures reported in [32], the continuous PAS are first estimated by filtering the actual power angular distributions of the propagation channel by a function that corresponds to a limited aperture of an antenna. The filtering is performed for both of the considered frequencies. Then, the both spectra are normalized to the sum power of unity such that they can be interpreted as probability distribution functions (PDFs). Finally, the total variation distance between the probability distributions, i.e., normalized PASs is calculated.

1) *Beam Filtering*: Any antennas or arrays can be used for defining the angular filter. It can be, for example, a phased array and the filtering operation would equal the classical Bartlett beamforming. Here, a simple synthetic radiation pattern $G(\Omega)$ specified by the 3GPP in [14, Table 7.3-1] is adopted. As shown in Fig. 6, the peak to minimum gain ratio is 30 dB and 10° is chosen as the definable HPBW θ_{3dB} . We take

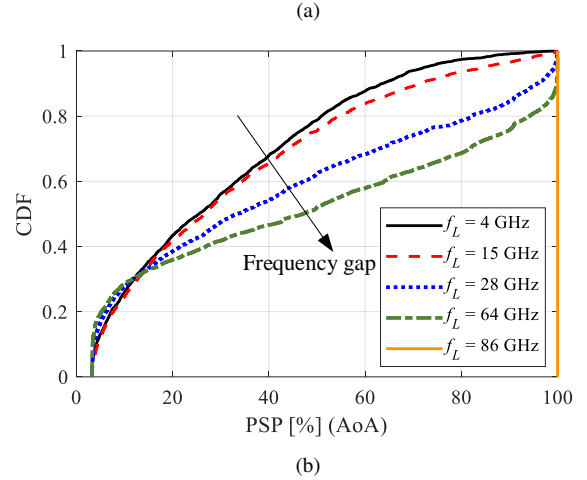
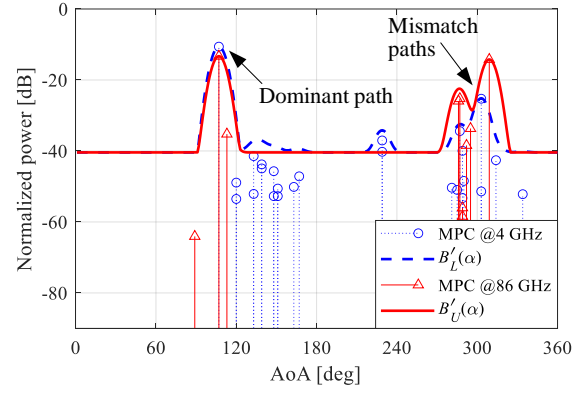


Fig. 7. (a) Normalized power patterns for PSP calculation (link 15). (b) Empirical CDF of the PSP metric with $f_U = 86$ GHz and $f_L = 4, 15, 28, 64, 86$ GHz.

convolution $\int P(\Omega) G(\alpha - \Omega) d\Omega$ of the propagation channel PAS $P(\Omega)$ and the angular filter $G(\Omega)$. This corresponds to steering the beam to a direction α and collecting the sum power from all observable MPCs weighted with corresponding beam gains. The resulting power with steering angle α is

$$\begin{cases} B_L(\alpha) = \sum_{p=1}^{l_L} P_{L,p} G(\alpha - \Omega_{L,p}) \\ B_U(\alpha) = \sum_{p=1}^{l_U} P_{U,p} G(\alpha - \Omega_{U,p}). \end{cases} \quad (2)$$

2) *Power Normalization*: Both estimated spectra are normalized to the sum power of unity such that they can be interpreted as PDFs. The normalized PAS at lower frequency is calculated as

$$B'_L(\alpha) = \frac{B_L(\alpha)}{\int B_L(\alpha) d\alpha} \quad (3)$$

The $B'_U(\alpha)$ is similarly defined with respect to the upper frequency PAS $B_U(\alpha)$. Fig. 7(a) depicts an example of normalized PAS $B'_L(\alpha)$ and $B'_U(\alpha)$ for link 15 at 4 GHz and 86 GHz, respectively. Compared with the multi-path shown in Fig. 5, the dominant directions of wave propagation in azimuth plane are aligned at the two frequencies, except for the path along the direction of 300° .

3) *Total Variation Calculation*: As defined in [32], the total variation distance between the normalized PASs is calculated as

$$d_{\text{tv}} = \frac{1}{2} \int |B'_L(\alpha) - B'_U(\alpha)| d\alpha. \quad (4)$$

The $d_{\text{tv}} \in [0, 1]$ characterizes the cumulative difference of normalized PASs between two frequency bands. Conversely, the PSP is defined as

$$S = (1 - d_{\text{tv}}) \cdot 100\% \quad (5)$$

The example link illustrated in Fig. 7(a) (and Fig. 5) yields PSP of 57.0%. We can observe how the deviation between $B'_L(\alpha)$ and $B'_U(\alpha)$ reduces the PSP value though the strongest path directions at both frequencies are perfectly aligned.

Empirical cumulative distribution function (CDF) of the PSP metric is collected over all 2875 links. In order to compare the spatial channel similarity across different frequency combinations, the CDF curves depicted in Fig. 7(b) are determined for five cases while keeping $f_U = 86$ GHz and choosing $f_L = 4, 15, 28, 64,$ and 86 GHz. Since in this particular comparison the beam pattern is unchanged across frequency bands, we would expect to get the higher PSP the smaller frequency gap $f_U - f_L$ we have. We can remark that the similarity percentage indeed increases in general with the decreasing frequency spacing between f_U and f_L and, ultimately, the similarity is always 100% at $f_U = f_L$, as anticipated. On the other hand, we can observe that this trend does not hold for all curves and even reverses when the PSP values are below 13%.

A low PSP value corresponds to significant difference between $B'_L(\alpha)$ and $B'_U(\alpha)$. This does not, however, necessarily mean high inaccuracy on beam directions obtained from out-of-band channel, as can be seen in the analysis of the next section concerning the example link shown in Fig 7(a) and 8(a). Moreover, the PSP metric only characterizes the overall channel gain difference over all directions in 360° azimuth plane, lacking the details at specific directions. Hence, the PSP metric can mainly be used to evaluate the channel similarity when multi-band channels have a high spatial congruence. We can summarize that the PSP provides information on angular multi-path, but it is not suitable for indicating the usefulness of out-of-band beam directions.

B. Beam Direction-Based Similarity Metric

To avoid the reverse results at different levels of channel similarity and to draw more practical conclusions, we define the other method with a focus on the collection of desired beam directions at the two frequencies. With this metric, we also consider the assumed antenna size constraints at different frequencies, rather than using the same beam pattern shown in Fig. 6.

Let us assume that low- and high-frequency radios and antenna systems operate equally at both link ends, where the lower frequency antenna system presumably has smaller electrical size, resulting in lower angular resolution and larger beam width of the main lobe. Next we identify two sets of best beam directions at low and high frequencies, using

the corresponding antenna beam patterns and propagation channel data. The sets of potential beam pointing angles in azimuth can be written as $\mathcal{A}_L = \{\theta_L | \theta_L \in [-\pi, \pi]\}$ and $\mathcal{A}_U = \{\theta_U | \theta_U \in [-\pi, \pi]\}$, respectively. Finally, we define a power ratio $R = \hat{P}_U(\mathcal{A}_L) / \hat{P}_U(\mathcal{A}_U)$ to measure how much potential channel gain is lost if the low-frequency beam direction information is used for high-frequency beam search instead of choosing its own channel information. Besides, we can count how many false, i.e., completely useless directions are provided from the low frequency for the high frequency.

1) *Determining Best Beam Directions*: The sets of best beam directions \mathcal{A}_L and \mathcal{A}_U depend on the underlying radio channel, i.e., propagation channel and antenna systems. By the best beam directions we mean a minimum set of directions for beam steering or antenna orientation, such that the potential multi-path channel gains can be maximally² utilized. Different gain patterns $G_L(\Omega)$ and $G_U(\Omega)$ are employed to filter the raw PADPs according to Eq. (2). Fig. 8(a) shows an example of filtered PAS $B_L(\alpha)$ and $B_U(\alpha)$ for the link 15 using the 3GPP beam shape with the HPBW of 40° and 10° at 4 GHz and 86 GHz, respectively. In [33], three methods are presented for identifying the desired directions. Here, the simplest method is utilized to choose the local maxima of $B(\alpha)$ with power threshold Δ_{th} of 15 dB. As shown in Fig. 8(a), in total two best beam directions (the black squares) are selected in lower band, while there are three directions selected in higher band. One more direction can be detected in 295° at 86 GHz because of narrower beam enabling to distinguish observable directions without angle ambiguities.

2) *Calculating Power Ratio and False Direction Number*: Based on the estimated sets of best beam directions, we consequently define the power ratio as the summation of power observed by the high frequency antenna over different steering angle sets

$$R = \frac{\hat{P}_U(\mathcal{A}_L)}{\hat{P}_U(\mathcal{A}_U)} = \frac{\sum_{\theta_L \in \mathcal{A}_L} B_U(\theta_L)}{\sum_{\theta_U \in \mathcal{A}_U} B_U(\theta_U)}. \quad (6)$$

The ratio R determines how much power is collected in the high-frequency case using different beam direction sets. Large R indicates less power loss using low-frequency channel information and higher spatial similarity between radio channels at the two frequencies.

A direction $\alpha \in \mathcal{A}_L$ proposed from low-frequency channel is interpreted as useless or “false” for high-frequency beam search if the high-frequency antenna does not collect any significant power when steered to that direction. More rigorously, we define the number of false directions as

$$N_f = \text{card} \left(\arg \frac{B_U(\alpha)}{\max_{\alpha' \in \mathcal{A}_U} B_U(\alpha')} < \Delta_P \right), \quad (7)$$

where $\text{card}(\cdot)$ denotes the cardinality of a set and Δ_P is a power threshold (e.g., -30 dB). The number of these false directions can be counted per link and their empirical probability distribution over all links can be extracted. Likewise,

²As is well known, the optimal selection of beam directions depends on transceiver architectures, MIMO transmission schemes, beamforming strategies, etc., and hence cannot be exactly determined without such a priori knowledge.

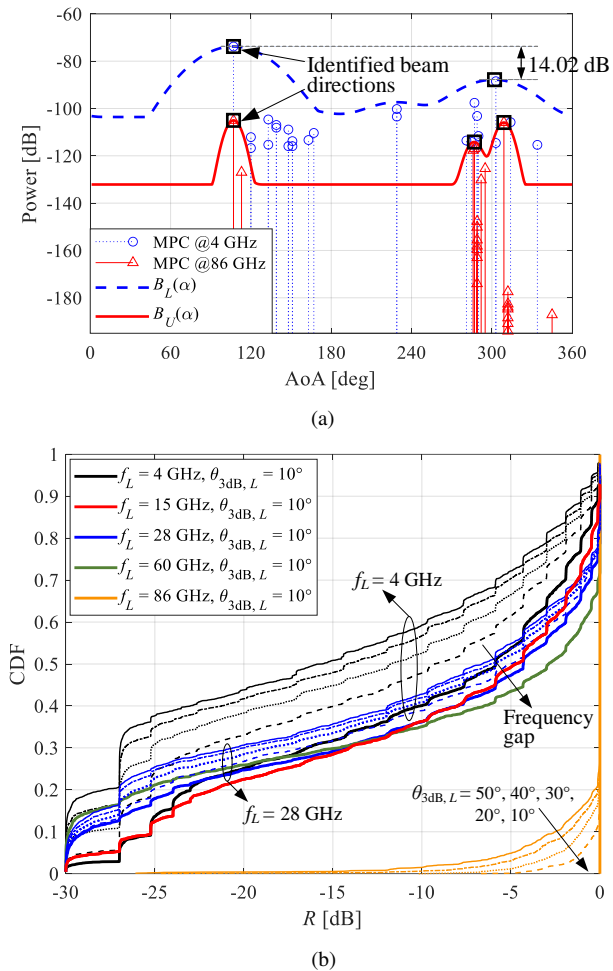


Fig. 8. (a) Original discrete PAS and filtered power patterns (link 15). (b) Empirical CDF of the power ratios R under different f_L and $\theta_{3\text{dB},L}$ combinations with respect to $f_U = 86$ GHz and $\theta_{3\text{dB},U} = 10^\circ$. Line types denote $\theta_{3\text{dB},L}$ values: solid 50° , dash dotted 40° , dotted 30° , dashed 20° , and solid bold 10° .

the cardinality of sets \mathcal{A}_L and \mathcal{A}_U can be collected and their corresponding PDF can be extracted. For the case shown in Fig. 8(a), the corresponding R and N_f are respectively -2.02 dB and 0, while if Δ_{th} was selected as 10 dB, R and N_f were -2.86 dB and 0, respectively.

It is evident that the power ratio R depends on both the similarity of discrete PASs $P_L(\Omega)$ and $P_U(\Omega)$, as well as the shapes of antenna patterns $G_L(\Omega)$ and $G_U(\Omega)$. For assessing the proposed method, we determine the CDF of R while keeping $f_U = 86$ GHz and the HPBW of G_U as 10° , and taking selected combinations of $f_L = 4, 15, 28, 64, 86$ GHz and the HPBW of G_L as $50^\circ, 40^\circ, 30^\circ, 20^\circ$, and 10° . We can observe from Fig. 8(b) that R almost monotonically increases, i.e., the power loss at high frequency by using the low-frequency spatial channel information becomes smaller, as both the frequency gap and the HPBW difference decrease. The highest loss is 30 dB, which is determined by the peak to minimum gain ratio of the selected 3GPP beam shapes shown in Fig. 6. As expected, when the same frequencies (i.e., $f_L = f_U$) and HPBW are selected, the power loss is 0 dB over all links (see the orange bold solid line). Moreover,

it seems that the beam width has even stronger impact on channel similarity than the frequency difference. For example, the power ratio is much larger when using the spatial channel information at $f_L = 4$ GHz with $\theta_{3\text{dB},L} = 10^\circ$ in comparison with the results at $f_L = 28$ GHz with $\theta_{3\text{dB},L} = 40^\circ$.

IV. RESULTS AND DISCUSSION

In the following, we evaluate the feasibility of out-of-band spatial channel information for mm-wave beam search based on the previously described multi-band propagation data, using the beam direction-based similarity metric defined in Section III-B. We choose upper/lower frequency combinations 4/86 GHz and 28/100 GHz for the simulation- and measurement-based analyses, respectively. Instead of the ideal 3GPP beam pattern, we utilize more practical beam patterns of uniform linear arrays (ULAs) with different element number N at different frequencies.

A. Validation with Dual-Band LOS Measurements

The 28 GHz and 84 GHz measured PASs are filtered with the beam patterns of half-wavelength spaced ULAs with 4 and 8 elements, respectively. Here, 4 and 8 are typical numbers of elements in azimuth for commercial mmWave systems. Beam patterns $G_L(\Omega)$ and $G_U(\Omega)$ of arrays are defined for $\Omega \in [-\pi/2, \pi/2]$ bore-sight half plane with all-zero phasing, while the back half plane $\Omega \in [-\pi, -\pi/2] \cup [\pi/2, \pi]$ is set to constant -60 dB gain. As shown in Fig. 9(a), the HPBW of main lobes are 26.2° and 12.8° for $G_L(\Omega)$ and $G_U(\Omega)$, respectively. The filtering of PAS by beam patterns is performed by rotating the patterns, not by setting various steering angles and using DFT weights, as would be the normal procedure with phased arrays. This approach is chosen since propagation paths are distributed over a wide sector of angles and in turn, we can remove the impact of ULA orientation on realized beam patterns.

The two methods proposed in [33] for identifying beam directions are used. With method 1 (M1) each local maximum of $B(\alpha)$ within $\Delta_{\text{th}} = 10$ dB range from the global maximum is selected, and for method 2 (M2), the same 10 dB range is used, but instead of local maxima the directions are selected based on the power and computational correlation between corresponding channel frequency responses.

Fig. 9(b) shows multi-path of an example link in the corridor environment. It can be observed that one beam direction at 28 GHz and two at 100 GHz can be extracted using M2 and the corresponding power loss is 0.91 dB ($= -R$ dB). When using M1, only one beam direction can be extracted at both frequencies and the resulting power loss is 1.55 dB. In a link of the entrance hall, depicted in Fig. 9(c), three beam directions can be detected at two frequency bands with power losses 0.13 dB and 0.09 dB using M1 and M2, respectively. The number of false directions N_f is zero in all mentioned cases. In general, M2 can estimate more possible beam directions than M1 [33], which leads to smaller power loss. This is the trend especially when using narrower beam pattern to filter the propagation channel. Measurement-based results show that our proposed metric performs well in LOS scenarios between two bands with tens of gigahertz frequency gap, especially when

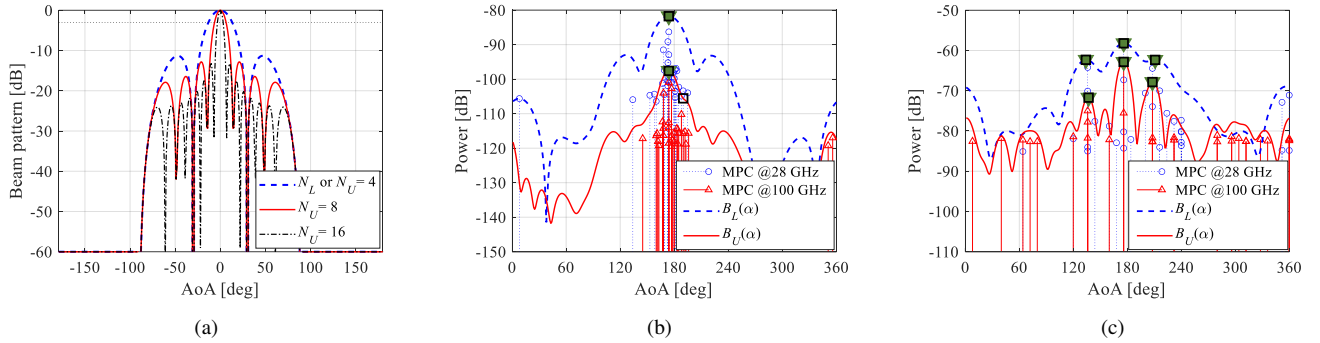


Fig. 9. (a) Beam patterns of 4-, 8-, and 16-element ULAs. Measurement-based analysis of spatial channel similarity between 28 GHz and 100 GHz in (b) indoor corridor and (c) entrance hall with $(N_L, N_U) = (4, 8)$. The green inverted triangles and black squares in (b) and (c) represent the identified beam directions using M1 and M2, respectively.

the more advanced beam identification method, i.e., M2 is adopted. We can observe that in LOS condition the angular profile of propagation channels are similar, the out-of-band information is useful, and the power loss due to incorrect beam directions at the upper frequency is minor.

B. Feasibility Study with Statistical Analysis

The evaluations of Section III-B show significant impact of antenna HPBW on the measure of spatial channel similarity across different frequencies using ideal 3GPP beam patterns. Here, we promote statistical analysis of radio channel similarity based on 4 GHz and 86 GHz ray tracing data, where ULA beam patterns are used to filter propagation channels. At f_L we use similar 4-element ULA as in the previous section, while at f_U we evaluate 4-, 8-, and 16-element ULAs. All three beam patterns are illustrated in Fig. 9(a).

CDF curves of power ratios R over all 2875 NLOS links assuming different beam patterns and beam direction estimation methods are shown in Fig. 10, as well as their statistics in Table III. As the first observation, we can notice that losses R are substantially higher as compared to the LOS examples of the previous section. Furthermore, we can observe that the CDF curves for M2 can provide slightly higher values of R compared with M1. The values of R are also sensitive to the beam width, i.e., the ULA aperture. When using the direction information of 4 GHz channel to aid in the 86 GHz beam search, at worst 2.27 dB, 7.31 dB, and 14.77 dB power losses are introduced in 50% of cases when 4-, 8-, and 16-element ULAs are employed in higher frequency bands, respectively.

While R indicates whether all significant directions are included in 86 GHz beam steering, it is also important to consider how many false directions are indicated by the 4 GHz \mathcal{A}_L . Fig. 11 depicts the PDFs of both the number of false directions N_f and all identified beam directions within \mathcal{A}_L . We have set in this analysis Δ_P of eq. (7) as -30 dB. As expected, less false directions are introduced if the same beam patterns are used at 4 GHz and 86 GHz.

With simple reasoning one can understand that statistically R and N_f must be proportional. Namely, if the criteria to find beam directions at f_L is loosened, the more directions are provided to f_U in the set \mathcal{A}_L (this is shown in [33]) and the higher ratio R is obtained, but consequently N_f is increased as

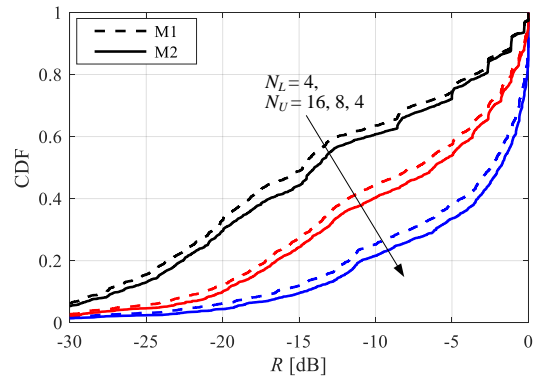


Fig. 10. Empirical CDF of the power ratio metric based on ray tracing simulation data. Black, red, and blue curves denote $N_U = 16, 8,$ and 4 cases, respectively.

TABLE III
THE STATISTICS OF POWER RATIOS R AND NUMBER OF FALSE DIRECTIONS N_f UNDER DIFFERENT ANTENNA CONFIGURATIONS WITH $\Delta_{th} = 10$ dB.

(N_L, N_U)		(4, 4)		(4, 8)		(4, 16)	
Method		M1	M2	M1	M2	M1	M2
R [-dB]	10%	16.49	14.7	21.14	20.00	27.58	26.77
	50%	2.27	1.88	7.31	6.20	14.77	14.00
	90%	0	0	0.26	0.21	1.13	1.12
N_f [%]	= 0	59.44	58.05	54.09	54.16	43.58	43.30
	≤ 1	89.62	85.18	86.47	83.17	80.77	75.48

well. In other words, the higher number of false directions we can tolerate, the lower power loss we can achieve when solely following the out-of-band directions. Hence, there is a trade-off between R and N_f when measuring the degree of spatial similarity between low- and high-frequency radio channels. It is remarkable that N_f is less than or equal to one in most of the cases ($>80\%$), meaning that spatial channel similarity between 4 GHz and 86 GHz radio channel can be exploited to realize coarse estimation of mm-wave beam directions without noticeable effort of searching around false directions.

C. Analysis of Non-Successful Cases

There is a good share of cases where the 4 GHz beam information provides an adequate basis for the 86 GHz beam

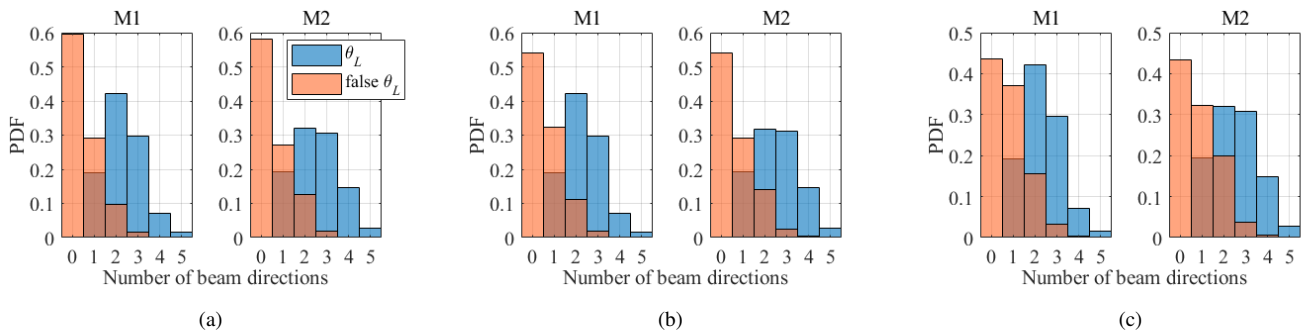


Fig. 11. Empirical PDF of the number of false directions and all extracted beam directions using 4 GHz out-of-band spatial channel information with the (N_L, N_U) of (a) (4, 4), (b) (4, 8), and (c) (4, 16).

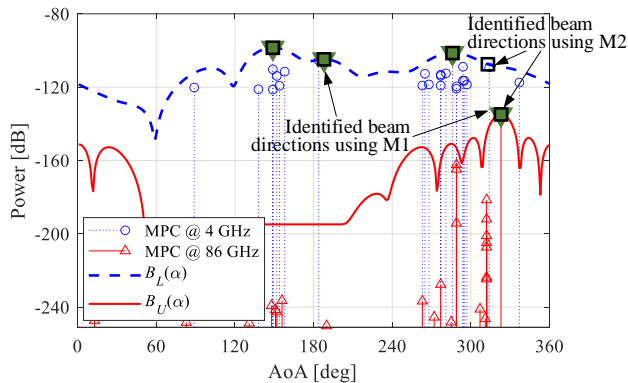


Fig. 12. Original discrete PAS and filtered power patterns (Link 19).

directions as the statistical analysis indicates. A good example is the link 15 shown in Fig. 8(a) with $N_f = 0$ and $R = -2.86$ dB. However, there is another set of links where low-frequency radio channel observed by a lower resolution antenna provides no useful information for 86 GHz beam search. In these cases there is often a strong path at the low frequency, which is not present or is only weak at the high frequency. We do not have an exhaustive analysis of all these incidences, but in some cases the root cause is diffraction and in some other cases the path is more severely shadowed by an obstacle at the high frequency. An example of such link is shown in Fig. 12 with $(N_L, N_U) = (4, 8)$, where $N_f = 2$ (with M1) and $R = -16.15$ dB. There the strong paths of 4 GHz channels do not coincide with those of 86 GHz channel, or more precisely, there is only a single dominant propagation path at 84 GHz and it is not present at 4 GHz.

Overall, the spatial similarity of propagation channel at different RFs can be assessed with the beam domain perspective. The out-of-band spatial channel information aided mm-wave beam search strategy is expected to perform well for the links containing strong and dominant paths, while multipath scattering components easily leads to angle mismatch between two well-separated frequency bands. The analysis of the measurement- and ray tracing-based results in LOS and NLOS scenarios, respectively, supports the expectation.

V. CONCLUSION

In this paper, we analyze an extensive set of multi-band propagation data and propose two metrics to evaluate the

spatial similarity of radio channels across different frequencies. We conduct a feasibility study of out-of-band spatial information aided mm-wave beam search from a radio channel similarity perspective. The first metric, the PAS similarity percentage, was found non satisfying. The other, the proposed beam direction-based spatial similarity metric compares the potential angular directions estimated from radio channels and provides the power loss and number of false direction introduced by solely using out-of-band information. Moreover, we perform a quantitative analysis of both point cloud ray tracing and measured data wrt. the metric. The results indicate that the usability of low-frequency radio channel information for high-frequency beam search evidently depends on many choices, e.g., of assumed angular resolutions and beam patterns of antennas, of the frequency gaps, of the criterion to select beam directions, and of accepting false directions. Overall, it seems practical to leverage available spatial channel information from lower frequency bands to aid mm-wave beam steering from the radio channel point of view, but it should not rely on out-of-band information blindly. For example, among the evaluated NLOS links, in 50% of cases one would lose 6.2 dB or less power, if 86 GHz beam steering with eight element ULA solely follows the out-of-band direction set \mathcal{A}_L obtained from 4 GHz radio channel with four element ULA, instead of the in-band direction set \mathcal{A}_U .

For future work, the need of high-efficient beam search strategies becomes even more urgent in upper mm-wave and terahertz bands (e.g., 100–300 GHz), since narrower beams increase the complexity of beam management under possible hardware limitations with potentially less flexibility. It would be of interest to include more statistical performance analysis of our proposed channel similarity metric with exhaustive directional propagation measurement campaigns. Moreover, developing a sophisticated metric for dynamic channel similarity measure is also an interesting research direction.

ACKNOWLEDGMENT

The authors would like to thank their colleague Mr. Yejian Lyu from Aalborg University for his valuable support in channel measurements and parameter estimation.

REFERENCES

- [1] H. Tataria, M. Shafi, A. F. Molisch, M. Dohler, H. Sjöland, and F. Tufvesson, “6G wireless systems: Vision, requirements, challenges,

- insights, and opportunities,” *Proc. IEEE*, vol. 109, no. 7, pp. 1166–1199, July 2021.
- [2] A. Pärssinen, M. Alouini, M. Berg, T. Kürner, P. Kyösti, M. Leinonen, M. Matinmikko-Blue, E. McCune, U. Pfeiffer, and P. Wambacq (eds.), “White paper on RF enabling 6G – opportunities and challenges from technology to spectrum,” White paper. 6G Research Visions, No. 13. University of Oulu, April 2021.
 - [3] K. Rikkinen, P. Kyösti, M. E. Leinonen, M. Berg, and A. Pärssinen, “THz radio communication: Link budget analysis toward 6G,” *IEEE Communications Magazine*, vol. 58, no. 11, pp. 22–27, Nov. 2020.
 - [4] G. R. MacCartney and T. S. Rappaport, “Rural macrocell path loss models for millimeter wave wireless communications,” *IEEE J. Sel. Areas Commun.*, vol. 35, no. 7, pp. 1663–1677, July 2017.
 - [5] P. Zhang, B. Yang, C. Yi, H. Wang, and X. You, “Measurement-based 5G millimeter-wave propagation characterization in vegetated suburban macrocell environments,” *IEEE Trans. Antennas Propag.*, vol. 68, no. 7, pp. 5556–5567, July 2020.
 - [6] J. Ko, Y.-J. Cho, S. Hur, T. Kim, J. Park, A. F. Molisch, K. Haneda, M. Peter, D.-J. Park, and D.-H. Cho, “Millimeter-wave channel measurements and analysis for statistical spatial channel model in in-building and urban environments at 28 GHz,” *IEEE Trans. Wireless Commun.*, vol. 16, no. 9, pp. 5853–5868, Sept. 2017.
 - [7] P. Zhang, H. Wang, and W. Hong, “Radio propagation measurements and cluster-based analysis for 5G millimeter-wave cellular systems in dense urban environments,” *Front. Inf. Technol. Electron. Eng.*, vol. 22, no. 4, pp. 471–487, Apr. 2021.
 - [8] M. Shafi *et al.*, “Microwave vs. millimeter-wave propagation channels: Key differences and impact on 5G cellular systems,” *IEEE Commun. Mag.*, vol. 56, no. 12, pp. 14–20, Dec. 2018.
 - [9] V. Raghavan, J. Cezanne, S. Subramanian, A. Sampath, and O. Koymen, “Beamforming tradeoffs for initial UE discovery in millimeter-wave MIMO systems,” *IEEE J. Sel. Topics Signal Process.*, vol. 10, no. 3, pp. 543–559, Apr. 2016.
 - [10] M. Giordani, M. Polese, A. Roy, D. Castor, and M. Zorzi, “A tutorial on beam management for 3GPP NR at mmWave frequencies,” *IEEE Commun. Surveys Tuts.*, vol. 21, no. 1, pp. 173–196, 1st Quart. 2019.
 - [11] N. González-Prelcic, A. Ali, V. Va, and R. W. Heath, “Millimeter-wave communication with out-of-band information,” *IEEE Commun. Mag.*, vol. 55, no. 12, pp. 140–146, Dec. 2017.
 - [12] A. Ali, N. González-Prelcic, and R. W. Heath, “Millimeter wave beam-selection using out-of-band spatial information,” *IEEE Trans. Wireless Commun.*, vol. 17, no. 2, pp. 1038–1052, Feb. 2018.
 - [13] D. Dupleich, R. Müller, M. Landmann, E.-A. Shinwasusin, K. Saito, J.-I. Takada, J. Luo, R. Thomä, and G. Del Galdo, “Multi-band propagation and radio channel characterization in street canyon scenarios for 5G and beyond,” *IEEE Access*, vol. 7, pp. 160 385–160 396, 2019.
 - [14] TR 38.901, “Study on channel model for frequencies from 0.5 to 100 GHz,” 3GPP, Tech. Rep. V14.1.1, July 2017.
 - [15] B. Peng, K. Guan, S. Rey, and T. Kürner, “Power-angular spectra correlation based two step angle of arrival estimation for future indoor terahertz communications,” *IEEE Trans. Antennas Propag.*, vol. 67, no. 11, pp. 7097–7105, Nov. 2019.
 - [16] W. Fan, I. Carton, J. Ø. Nielsen, K. Olesen, and G. F. Pedersen, “Measured wideband characteristics of indoor channels at centimetric and millimetric bands,” *EURASIP J. Wireless Commun. Netw.*, vol. 58, 2016.
 - [17] P. Zhang, J. Li, H. Wang, H. Wang, and W. Hong, “Indoor small-scale spatiotemporal propagation characteristics at multiple millimeter-wave bands,” *IEEE Antennas Wireless Propag. Lett.*, vol. 17, no. 12, pp. 2250–2254, Dec. 2018.
 - [18] P. Zhang, J. Li, H. Wang, and X. You, “Millimeter-wave space-time propagation characteristics in urban macrocell scenarios,” in *Proc. IEEE Int. Conf. Commun. (ICC)*, Shanghai, China, May 2019, pp. 1–6.
 - [19] Y. Lyu, P. Kyösti, and W. Fan, “Sub-THz VNA-based channel sounder structure and channel measurements at 100 and 300 GHz,” in *Proc. IEEE Int. Symp. Pers., Indoor Mobile Radio Commun. (PIMRC)*, Helsinki, Finland, Sept. 2021, pp. 1–5.
 - [20] S. L. H. Nguyen *et al.*, “On the frequency dependency of radio channel’s delay spread: Analyses and findings from mmMAGIC multi-frequency channel sounding,” in *Proc. Eur. Conf. Antennas Propag. (EuCAP)*, London, UK, Apr. 2018, pp. 1–5.
 - [21] mmMAGIC D2.2, “Measurement results and final mmMAGIC channel models,” *Deliverable D2.2, ver. 1.* (<https://5g-mmmagic.eu/results/>), 2017.
 - [22] C. Yi, P. Zhang, H. Wang, and W. Hong, “Multipath similarity index measure across multiple frequency bands,” *IEEE Wireless Commun. Lett.*, vol. 10, no. 8, pp. 1677–1681, Aug. 2021.
 - [23] P. Koivumäki, G. Steinböck, and K. Haneda, “Impacts of point cloud modeling on the accuracy of ray-based multipath propagation simulations,” *IEEE Trans. Antennas Propag.*, vol. 69, no. 8, pp. 4737–4747, Aug. 2021.
 - [24] J. Järveläinen, A. Karttunen, and K. Haneda, “Indoor propagation channel simulations at 60 GHz using point cloud data,” *IEEE Trans. Antennas Propag.*, vol. 64, no. 8, pp. 4457–4467, Aug. 2016.
 - [25] Zoller+Fröhlich GmbH, “Z+F IMAGER@5006h,” 2010. [Online]. Available: https://zf-usa.com/wp-content/uploads/2011/10/IMAGER\5006h_brochure.pdf
 - [26] J. Vehmas, J. Jarvelainen, S. L. H. Nguyen, R. Naderpour, and K. Haneda, “Millimeter-wave channel characterization at helsinki airport in the 15, 28, and 60 GHz bands,” in *Proc. IEEE 84th Veh. Technol. Conf. (VTC-Fall)*, Montreal, QC, Canada, Sep. 2016, pp. 1–5.
 - [27] J. Järveläinen, S. L. H. Nguyen, K. Haneda, R. Naderpour, and U. T. Virk, “Evaluation of millimeter-wave line-of-sight probability with point cloud data,” *IEEE Wireless Commun. Lett.*, vol. 5, no. 3, pp. 228–231, June 2016.
 - [28] P. Koivumäki, A. F. Molisch, and K. Haneda, “Line-of-sight probability in cluttered urban microcells: Analyses using poisson point process and point cloud,” *IEEE Trans. Antennas Propag.*, vol. 70, no. 3, pp. 2161–2173, Mar. 2022.
 - [29] A. W. Mbugua, W. Fan, K. Olesen, X. Cai, and G. F. Pedersen, “Phase-compensated optical fiber-based ultrawideband channel sounder,” *IEEE Trans. Microw. Theory Techn.*, vol. 68, no. 2, pp. 636–647, Feb. 2020.
 - [30] Y. Lyu, A. W. Mbugua, K. Olesen, P. Kyösti, and W. Fan, “Design and validation of the phase-compensated long-range sub-THz VNA-based channel sounder,” *IEEE Antennas Wireless Propag. Lett.*, vol. 20, no. 12, pp. 2461–2465, Dec. 2021.
 - [31] M. Li, F. Zhang, Y. Ji, and W. Fan, “Virtual antenna array with directional antennas for millimeter-wave channel characterization,” *IEEE Trans. Antennas Propag.*, vol. 70, no. 8, pp. 6992–7003, Aug. 2022.
 - [32] P. Kyösti, L. Hentilä, W. Fan, J. Lehtomäki, and M. Latva-Aho, “On radiated performance evaluation of massive MIMO devices in multiprobe anechoic chamber OTA setups,” *IEEE Trans. Antennas Propag.*, vol. 66, no. 10, pp. 5485–5497, Oct. 2018.
 - [33] P. Kyösti, M. F. De Guzman, K. Haneda, N. Tervo, and A. Pärssinen, “How many beams does sub-THz channel support?” *IEEE Antennas Wireless Propag. Lett.*, vol. 21, no. 1, pp. 74–78, Jan. 2022.



Pekka Kyösti received the M.Sc. degree in mathematics and the D.Sc. (Hons.) in communications engineering from the University of Oulu, Finland, in 2000 and 2018, respectively. He is currently a research director in 6G Flagship programme and a docent (adjunct professor) with the Centre for Wireless Communications (CWC), University of Oulu, and a senior specialist with Keysight Technologies Finland Oy. His present activities are radio channel characterization for 6G systems, and channel modelling and over-the-air emulation for 5G systems.

From 1998 to 2002, he was with Nokia Networks, from 2002 to 2016, he was with Elektrobit/Anite, from 2016 onward he has been with Keysight (part time). Since 2002, he has been involved in radio channel measurements, estimation and modelling. From 2008 to 2012, he was actively developing methods for MIMO over-the-air testing. He has acted in contributor and task leader roles in many past research projects such as, e.g., WINNER (I,II,+) and METIS. He has also contributed on channel modelling on many standardization fora such as ITU-R, 3GPP (RAN1, RAN4), CTIA, and IEEE 802. He has been a guest editor in special issues of IET Microwaves, Antennas & Propagation, IEEE JSAC, IEEE Access, IEEE OJAP, and IEEE T-AP, in years 2019–2024.



Peize Zhang (Member, IEEE) received the B.S. degree from the Beijing University of Posts and Telecommunications, China, in 2015, the M.S. degree from the China Academy of Telecommunications Technology, Beijing, China, in 2018, and the Ph.D. degree from Southeast University, Nanjing, China, in 2022, all in electrical engineering.

From 2016 to 2018, he was also a research assistant with the China Academy of Information and Communications Technology, Beijing, China. In 2021, he was a visiting Ph.D. student with the

Université Catholique de Louvain, Louvain-la-Neuve, Belgium. Since 2022, he has been a Post-Doctoral Researcher in 6G Flagship programme with the Centre for Wireless Communications (CWC), University of Oulu, Finland. His current research interests focus on propagation, deployment, and performance issues of millimeter-wave/THz communication systems.



Aarno Pärssinen (Senior Member, IEEE) received the M.Sc., Licentiate in Technology and Doctor of Science degrees in electrical engineering from the Helsinki University of Technology, Finland, in 1995, 1997, and 2000, respectively.

From 1994 to 2000 he was with Electronic Circuit Design Laboratory, Helsinki University of Technology, Finland, working on direct conversion receivers and subsampling mixers for wireless communications. In 1996, he was a Research Visitor at the University of California at Santa Barbara. From

2000 to 2011 he was with Nokia Research Center, Helsinki, Finland. During 2009–2011 he served as a member of Nokia CEO Technology Council. From 2011 to 2013, he was at Renesas Mobile Corporation, Helsinki, Finland working as a Distinguished Researcher and RF Research Manager. From October 2013 to September 2014, he was an Associate Technical Director at Broadcom, Helsinki, Finland. Since September 2014 he has been with the Centre for Wireless Communications, University of Oulu, Oulu, Finland, where he is currently a Professor. He leads Devices and Circuits research area in 6G Flagship program financed by Academy of Finland. His research interests include wireless systems and transceiver architectures for wireless communications with special emphasis on the RF and analog integrated circuit and system design.

Aarno Pärssinen has authored and co-authored one book, two book chapters, more than 200 international journal and conference papers and holds several patents. He is a recipient of European Microwave Prize on the best paper of the European Microwave conference 2020. He is also one of the original contributors to Bluetooth low energy extension, now called as BT LE. He served as a member of the technical program committee of Int. Solid-State Circuits Conference in 2007–2017, where he was the chair of European regional committee in 2012–13, and the chair of the wireless sub-committee in 2014–2017. He has been serving as Solid-State Circuits Society representative for IEEE 5G initiative in 2015–2019.



Katsuyuki Haneda (Member, IEEE) is an associate professor in Aalto University School of Electrical Engineering, Espoo, Finland. He was an author and co-author of a number of best paper and student paper awards in the IEEE Vehicular Technology Conference and European Conference on Antennas and Propagation, among others. He also received the R. W. P. King paper award of the IEEE Transactions on Antennas and Propagation in 2021, together with Dr. Usman Virk. Dr. Haneda was an associate editor of the IEEE Transactions on Antennas and Propagation

between 2012 and 2016, and of an editor of the IEEE Transactions on Wireless Communications between 2013 and 2018. He was a guest editor of Special Issues on Antennas and Propagation Aspects of In-Band Full-Duplex Applications and on Artificial Intelligence in Radio Propagation for Communications in the IEEE Transactions on Antennas and Propagation in 2021 and 2022, respectively. He is also a guest editor of the forthcoming Special Section on Sub-THz and THz Radio Propagation: Measurements and Characterization in the IEEE Open Journal of Antennas and Propagation. He was a co-chair of a disciplinary working group on radio channels in European COST Actions CA15104 Inclusive Radio Communication Networks for 5G and beyond (IRACON) between 2016 and 2020. Dr. Haneda is a technical programme committee co-chair of the 17th European Conference on Antennas and Propagation (EuCAP 2023), Florence, Italy. His current research activity covers high-frequency radios such as millimeter-wave and beyond and wireless for medical and smart-city applications.



Pasi Koivumäki (Member, IEEE) received the M.Sc. (Tech.) (Hons.) degree from Aalto University School of Electrical Engineering, Espoo, Finland in 2017, where he is currently pursuing a D.Sc. (Tech.) in radio engineering. His current research activities include multi-band radio channel measurements, simulations and modeling focusing on mm-wave frequencies for 5G systems and beyond. His particular interests lie in ray-launching and ray-tracing algorithms for propagation and channel modeling in urban environments of future smart cities and their

combined effects on cellular coverage and quality of service.



Wei Fan (Senior Member, IEEE) received the B.Eng. degree from the Harbin Institute of Technology, Harbin, China, in 2009, the dual master's degree (Hons.) from the Politecnico di Torino, Turin, Italy, and the Grenoble Institute of Technology, Grenoble, France, in 2011, and the Ph.D. degree from Aalborg University, Aalborg, Denmark, in 2014. From February 2011 to August 2011, he was with Intel Mobile Communications, Aalborg, as a Research Intern. He conducted a three-month internship at Anite Telecoms oy (now Keysight Technologies),

Oulu, Finland, in 2014. He is currently an Associate Professor with Aalborg University, heading the “wireless channel and over-the-air testing” research group and a docent with University of Oulu, Finland. His main research interests include over-the-air testing of multiple antenna systems, radio channel sounding, modeling and emulation, and antenna array signal processing.